

3D Quasiconformal Representation and Solver

Qiguang Chen* and Lok Ming Lui*

Abstract. The analysis of mapping relationships and distortions in multidimensional data poses a significant challenge in contemporary research. While Beltrami coefficients offer a precise description of distortions in two-dimensional mappings, current tools lack this capability in the context of three-dimensional space. This paper presents a novel approach: a 3D quasiconformal representation that captures the local dilation of 3D mappings, along with an algorithm that establishes a connection between this representation and the corresponding mapping. Experimental results showcase the algorithm's effectiveness in eliminating foldings in 3D mappings, as well as in mapping reconstruction and generation. These features bear a resemblance to the 2D Linear Beltrami Solver technique. The work presented in this paper offers a promising solution for the precise analysis and adjustment of distortions in 3D data and mappings.

Key words. Quasiconformal mapping, Beltrami coefficient, 3D quasiconformal representation, Folding elimination, 3D Linear Beltrami Solver

1. Introduction. In modern scientific research, one of the main motivations is to process the vast amount of information encountered by human beings. This information includes 1D, 2D, and 3D data, which we encounter daily. Acoustic algorithms have been developed to process 1D information such as voice, while image data captured by cameras, rendered in games, and used in medical scenarios, such as X-ray images, are examples of 2D data. In mathematics, we consider surfaces on a 3D object as 2D and typically parameterize them on the 2D plane for further processing. 3D information includes MRI from brain, CT scans for chest, etc.

When analyzing relationships between pairs or groups of objects, we often use mappings to represent these relationships. However, when working with mappings, it's important to be mindful of the distortion that can arise from numerical implementations. In the 2D case, Beltrami coefficients, which are based on the Beltrami equation, can be used to measure the distortion of 2D mappings effectively. By controlling or analyzing the Beltrami coefficients of mappings, we can perform registration or shape analysis. However, this approach only works for 2D space. Unfortunately, we currently lack such an effective tool to describe distortion in 3D space precisely.

For a long time, we had no efficient way to reconstruct mappings from Beltrami coefficients. Obtaining Beltrami coefficients from mappings is straightforward, but the inverse direction is not explicitly defined in the Beltrami equation. However, the Linear Beltrami Solver (LBS) [18] has tackled this problem by providing an effective link between Beltrami coefficients and mappings. LBS has been successful in the field of mapping distortion adjustment, enabling the adjustment of distortion in both forward and backward directions. Various algorithms based on LBS have been proposed to solve challenging problems such as efficient parameterization, image registration, segmentation, retargeting, deturbulence, Teichmuller mapping, and har-

*Department of Mathematics, The Chinese University of Hong Kong, Shatin, Hong Kong (qgchen@math.cuhk.edu.hk, lmlui@math.cuhk.edu.hk).

monic Beltrami signature. Recently, some learning-based methods have been developed based on LBS, leveraging prior knowledge from data and the topological preservation advantages of LBS to effectively address challenging tasks and outperform conventional methods in various aspects.

However, LBS is theoretically based on the Beltrami equation, which can only provides a relationship between Beltrami coefficients and mappings in 2D space. when dealing with distortions in 3D space, LBS and its related efficient algorithms cannot be generalized for use in three dimensions. Unlike in 2D space, there is no quasiconformal representation similar to Beltrami coefficients in 3D space, nor is there an equation that relates this representation to its corresponding mapping.

In this paper, we propose a 3D quasiconformal representation that can effectively describe the local dilation of a 3D mapping and an algorithm similar to LBS, connecting this representation and its corresponding mapping. We also demonstrate that this algorithm can be used to eliminate foldings that appear in mappings, which is another important advantage of LBS. Experimental results show the effectiveness of this algorithm.

2. Contributions. The main contributions of this paper are outlined as follows.

1. We propose an effective 3D quasiconformal representation to describe the local dilation of 3D mappings.
2. We derive a partial differential equation that connects the proposed 3D quasiconformal representation and its corresponding mapping. Similar to LBS, this PDE can be discretized into an $N^3 \times N^3$ linear system, and boundary conditions and landmarks can be imposed easily.
3. Based on the above algorithm, we propose a simple but effective way to control distortion and eliminate foldings.
4. We carried out experiments demonstrating the above algorithm's effectiveness.

3. Related works. The computational method of conformal mapping [10, 17] has proven to be highly beneficial in the field of computer graphics. After the groundbreaking study by Gu et al. [11], there has been significant progress in using the conformal geometry framework for surface processing tasks. The work of Zayer, Rossl, and Seidel [30] already contains implicit generalizations of these ideas. Lui and his coauthors proposed the quasi-conformal extension of the surface registration framework, which includes the map compression [21] and the Linear Beltrami Solver (LBS) introduced in [18]. This solver has been used to develop fast spherical and disk conformal parameterization techniques [8, 9], as well as various registration algorithms for different applications [4, 13, 14, 15, 16, 19, 20, 22, 23, 26, 28, 29, 31, 36, 37, 32]. Additionally, LBS has been utilized in various segmentation algorithms for different applications [2, 27, 33, 35]. Besides, it has also been applied to shape analysis [1, 3, 6, 7, 24, 25]. However, due to the limitation of the quasiconformal theory the LBS is based on, these useful techniques have not been generalized to process 3D data. Learning-based methods based on LBS [5, 12] were also proposed to perform topology-preserving registration in the 2D space.

Some efforts have been made to apply the quasiconformal theory to process data with higher dimensions. In [34], a generalized conformality distortion is first defined to measure the dilatation of a n-dimensional quasiconformal map, after which optimization algorithms

are proposed to solve for various problems. Although these algorithms are effective, the generalized conformality distortion cannot represent the dilation precisely. In other words, it is not an equivalent quantity to the Beltrami coefficient in the higher dimension. Also, it is impossible to obtain the mappings from the defined quantity.

4. Mathematical background. In the following sections, we will introduce the Mathematical background for this paper. It includes two parts, polar decomposition for decomposing rotation and dilation, and quasiconformal mapping in the 2D space.

4.1. Polar decomposition. In this paper, we focus solely on the left polar decomposition for real rectangular matrices. We begin by denoting the set of $n \times n$ matrices over the field of real numbers as \mathcal{M}_n . The left polar decomposition of a matrix $A \in \mathcal{M}_n$ is a factorization of the form $A = UP$, where the columns of the matrix $U \in \mathcal{M}_n$ form an orthonormal basis, and $P \in \mathcal{M}_n$ is a symmetric positive semi-definite matrix. Specifically, $P = \sqrt{A^T A}$.

To better understand this definition, we first note that $A^T A$ is a symmetric semi-definite matrix. By applying the eigenvalue decomposition to this matrix, we obtain the form VDV^{-1} , where V is an orthogonal matrix because $A^T A$ is symmetric, and $V^{-1} = V^T$. The diagonal matrix D contains the eigenvalues of $A^T A$. After taking the square root of D , we obtain a matrix Σ containing the singular values of A . Thus, we have $P = \sqrt{A^T A} = W\Sigma W^T$.

Therefore, any linear transformation $T : \mathbb{R}^n \rightarrow \mathbb{R}^n$ is a composition of a rotation/reflection and a dilation.

For any matrix A and vector v , we have

$$(4.1) \quad \begin{aligned} \|Av\|^2 &= \langle Av, Av \rangle = \langle v, A^T Av \rangle = \langle v, \sqrt{A^T A} \sqrt{A^T A} v \rangle \\ &= \langle \sqrt{A^T A} v, \sqrt{A^T A} v \rangle = \|\sqrt{A^T A} v\|^2 \end{aligned}$$

from above, we know that the two norms are the same up to a rotation and/or a reflection.

4.2. Quasiconformal Mappings and Beltrami Coefficients. A surface with a conformal structure is known as a *Riemann surface*. Given two Riemann surfaces M and N , a map $f : M \rightarrow N$ is conformal if it preserves the surface metric up to a multiplicative factor called the conformal factor. Quasiconformal maps are a generalization of conformal maps that are orientation-preserving diffeomorphisms between Riemann surfaces with bounded conformal distortion, meaning that their first-order approximation maps small circles to small ellipses of bounded eccentricity (as shown in Figure 1).

Mathematically, a map $f : \mathbb{C} \rightarrow \mathbb{C}$ is quasiconformal if it satisfies the Beltrami equation $\frac{\partial f}{\partial \bar{z}} = \mu(z) \frac{\partial f}{\partial z}$, for some complex valued functions μ with $\|\mu\|_\infty < 1$ called the *Beltrami coefficient*. In particular, f is conformal around a small neighborhood of p if and only if $\mu(p) = 0$. f may be considered as a map composed of a translation to $f(p)$ followed by a stretch map $S(z) = z + \mu \bar{z}$, which is postcomposed by a multiplication of $f_z(p)$, which is conformal. All the conformal distortion of $S(z)$ is caused by $\mu(p)$. In other words, $S(z)$ is responsible for causing f to map small circles to small ellipses. By denoting $z = \rho + i\tau$ and $\mu = re^{i\theta}$, where $r = |\mu|$, and representing $S(z) = z + \mu \bar{z}$ in a matrix form, we have

$$(4.2) \quad \left[\begin{pmatrix} 1 & 0 \\ 0 & 1 \end{pmatrix} + r \begin{pmatrix} \cos \theta & -\sin \theta \\ \sin \theta & \cos \theta \end{pmatrix} \begin{pmatrix} 1 & 0 \\ 0 & -1 \end{pmatrix} \right] \begin{pmatrix} \rho \\ \tau \end{pmatrix} = \begin{pmatrix} 1 + r \cos \theta & r \sin \theta \\ r \sin \theta & 1 - r \cos \theta \end{pmatrix} \begin{pmatrix} \rho \\ \tau \end{pmatrix}$$

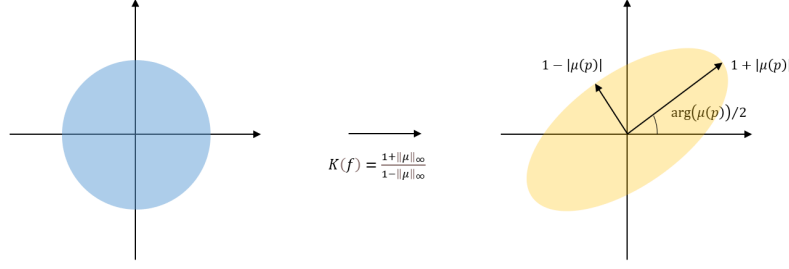


Figure 1: Illustration of how Beltrami equation μ measures the distortion of a quasiconformal mapping f that maps a small circle to an ellipse with dilation K

One can check that the eigenvalues for this matrix are $1 + |\mu|$ and $1 - |\mu|$. The eigenvectors for this matrix are $(\cos(\theta/2), \sin(\theta/2))^T$ and $(\cos((\theta - \pi)/2), \sin((\theta - \pi)/2))^T$ respectively. It is worth noting that the two eigenvectors are orthogonal to each other. The distortion or dilation can be measured by $K = (1 + |\mu|)/(1 - |\mu|)$. Thus the Beltrami coefficient μ gives us important information about the properties of a map.

5. Proposed algorithm. In this section, we describe the proposed algorithms in detail. We first focus on diffeomorphic mappings, which are invertible and do not produce overlaps or folds. We introduce the 3D quasiconformal representation for diffeomorphisms and derive a fast reconstruction algorithm, called the 3D quasiconformal solver, to reconstruct mappings from their representation. We then extend the 3D quasiconformal representation to describe the non-diffeomorphic mappings. Finally, we present an algorithm to eliminate foldings that appear in non-diffeomorphic mappings and ensure diffeomorphism.

5.1. Diffeomorphism. In this section, our primary focus is on diffeomorphism. To do this, we begin by extending the Beltrami coefficients to 3D space. Since there is no Beltrami equation for 3D space, we refer to these extended coefficients as 3D quasiconformal representation. Next, we derive an elliptic partial differential equation that relates the mappings to their 3D quasiconformal representation. Finally, from a discrete perspective, we discretize the equation to obtain a linear system. By solving this system with appropriate boundary conditions, we can reconstruct mappings from their representation.

5.1.1. 3D quasiconformal representation. Let X and Y be oriented, simply connected open subsets of \mathbb{R}^3 . Suppose we have a diffeomorphism $f : X \rightarrow Y$. The Jacobian matrix of f at a point p in X is denoted by $D_f(p)$. Since f is diffeomorphic, it is invertible. As a result, the Jacobian determinant $\det(D_f(p))$ is always positive for every point p in X .

Let Σ be the diagonal matrix containing the singular values a, b and c of $D_f(p)$, where by convention, we require that $a \geq b \geq c$. By polar decomposition, we have

$$(5.1) \quad D_f(p) = U(p)P(p) = U(p)\sqrt{D_f(p)^T D_f(p)} = UW\Sigma W^T = U\tilde{W}\Sigma\tilde{W}^T$$

where U is a rotation matrix, because the determinant of $D_f(p)$ and $P(p)$ are greater than 0,

implying that $\det(U(p)) = 1$. The matrix W contains eigenvectors for dilation, and a, b and c are the eigenvalues of $P(p)$ representing the dilation information. Hence they can be used to reconstruct the map. Furthermore, it is possible to represent the matrix W by Euler angles. To do so, we require that the column vectors of W form an orthonormal basis, and $\det(W) = 1$. However, the $\det(W)$ is not necessarily positive, meaning that W may not be a rotation matrix. This can be fixed by randomly multiplying a column of W by -1 to get a matrix \tilde{W} . This modification ensures $\det(\tilde{W}) = 1$, indicating that \tilde{W} is a rotation matrix, while at the same time the matrix $P(p)$ will not be changed. To see this, the matrix $P(p)$ can be reorganized as $aw_1w_1^T + bw_2w_2^T + cw_3w_3^T$, where w_1, w_2 and w_3 are the column vectors of W . Let $\tilde{w}_1 = -w_1$, then $\tilde{w}_1\tilde{w}_1^T = w_1w_1^T$. Thus reversing the direction of w_1 makes no change to $P(p)$. This also holds for w_2 and w_3 . Since this step is trivial, for simplicity, when we use W later in this paper, we assume $\det(W) = 1$ and it is a rotation matrix.

As is known, a rotation matrix R can be written in the following form:

$$(5.2) \quad \begin{aligned} R &= R_z(\theta_z)R_y(\theta_y)R_x(\theta_x) = \begin{pmatrix} \cos \theta_z & -\sin \theta_z & 0 \\ \sin \theta_z & \cos \theta_z & 0 \\ 0 & 0 & 1 \end{pmatrix} \begin{pmatrix} \cos \theta_y & 0 & \sin \theta_y \\ 0 & 1 & 0 \\ -\sin \theta_y & 0 & \cos \theta_y \end{pmatrix} \begin{pmatrix} 1 & 0 & 0 \\ 0 & \cos \theta_x & -\sin \theta_x \\ 0 & \sin \theta_x & \cos \theta_x \end{pmatrix} \\ &= \begin{pmatrix} \cos \theta_z \cos \theta_y & \cos \theta_z \sin \theta_y \sin \theta_x - \sin \theta_z \cos \theta_x & \cos \theta_z \sin \theta_y \cos \theta_x - \sin \theta_z \sin \theta_x \\ \sin \theta_z \cos \theta_y & \sin \theta_z \sin \theta_y \sin \theta_x + \cos \theta_z \cos \theta_x & \sin \theta_z \sin \theta_y \cos \theta_x - \cos \theta_z \sin \theta_x \\ -\sin \theta_y & \cos \theta_y \sin \theta_x & \cos \theta_y \cos \theta_x \end{pmatrix} \\ &= \begin{pmatrix} r_{11} & r_{12} & r_{13} \\ r_{21} & r_{22} & r_{23} \\ r_{31} & r_{32} & r_{33} \end{pmatrix} \end{aligned}$$

Then we obtain the Euler angles θ_x, θ_y and θ_z by

$$(5.3) \quad \begin{aligned} \theta_x &= \text{atan2}(r_{32}, r_{33}) \\ \theta_y &= \text{atan2}(-r_{31}, \sqrt{r_{32}^2 + r_{33}^2}) \\ \theta_z &= \text{atan2}(r_{21}, r_{11}) \end{aligned}$$

We define $(a, b, c, \theta_x, \theta_y, \theta_z)$ as the 3D quasiconformal representation for the mapping f at point p .

5.1.2. The PDE in the continuous case. By 5.1, we have

$$\det(D_f(p)) = \det(\sqrt{D_f(p)^T D_f(p)}) = abc$$

Recall the assumption that f is a diffeomorphism, implying $\det(D_f(p)) > 0$. Therefore, $D_f(p)^T D_f(p)$ is a symmetric positive definite matrix, and it can be written as

$$(5.4) \quad D_f(p)^T D_f(p) = \det(D_f(p))^{\frac{2}{3}} Q(p) = (abc)^{\frac{2}{3}} W \begin{pmatrix} \frac{a^2}{(abc)^{\frac{2}{3}}} & 0 & 0 \\ 0 & \frac{b^2}{(abc)^{\frac{2}{3}}} & 0 \\ 0 & 0 & \frac{c^2}{(abc)^{\frac{2}{3}}} \end{pmatrix} W^T$$

where $Q : \mathbb{R}^3 \rightarrow S(3)$, $S(3) = \{M \in S_{++} : \det(M) = 1\}$, S_{++} denotes the space of symmetric positive definite 3×3 matrices. Note that $\det(D_f(p))^{\frac{2}{3}}$ can be regarded as a diagonal matrix equal to $(abc)^{\frac{2}{3}}$ times an identity matrix, and the determinant of this matrix is $(abc)^2$, which is equal to $\det(D_f(p)^T D_f(p))$.

Right multiplying by $D_f(p)^{-1}$ on both side of the above equation, we have

$$(5.5) \quad D_f(p)^T = W \begin{pmatrix} a^2 & 0 & 0 \\ 0 & b^2 & 0 \\ 0 & 0 & c^2 \end{pmatrix} W^{-1} \frac{1}{\det(D_f(p))} C = W \begin{pmatrix} \frac{a}{bc} & 0 & 0 \\ 0 & \frac{b}{ac} & 0 \\ 0 & 0 & \frac{c}{ab} \end{pmatrix} W^{-1} C$$

where C is the adjugate matrix of $D_f(p)$ of the form

$$(5.6) \quad C = \begin{pmatrix} v_y w_z - v_z w_y & -u_y w_z + u_z w_y & u_y v_z - u_z v_y \\ -v_x w_z + v_z w_x & u_x w_z - u_z w_x & -u_x v_z + u_z v_x \\ v_x w_y - v_y w_x & -u_x w_y + u_y w_x & u_x v_y - u_y v_x \end{pmatrix} = \begin{pmatrix} \nabla v \times \nabla w & \nabla w \times \nabla u & \nabla u \times \nabla v \\ | & | & | \\ | & | & | \\ | & | & | \end{pmatrix}$$

where ∇u , ∇v and ∇w are the columns of $D_f(p)^T$.

Moving the terms before the matrix C on the right-hand side of Equation 5.5 to the left, we have

$$(5.7) \quad W \begin{pmatrix} \frac{bc}{a} & 0 & 0 \\ 0 & \frac{ac}{b} & 0 \\ 0 & 0 & \frac{ab}{c} \end{pmatrix} W^{-1} D_f(p)^T = C$$

Let A be a matrix defined as

$$(5.8) \quad A = W \begin{pmatrix} \frac{bc}{a} & 0 & 0 \\ 0 & \frac{ac}{b} & 0 \\ 0 & 0 & \frac{ab}{c} \end{pmatrix} W^{-1}$$

Given a domain of definition for a given function f , we can compute the matrix C for each point in the domain. Since each column vector in C is defined on each point in the domain of f , we can say that each column vector forms a vector field, and the same holds for the second and third column vectors. By examining the divergence of these three vector fields, we can confirm that they all have a divergence of 0. From another point of view, we can rewrite Equation 5.7 in the following form

$$(5.9) \quad A \begin{pmatrix} | & | & | \\ \nabla u & \nabla v & \nabla w \\ | & | & | \end{pmatrix} = \begin{pmatrix} \nabla v \times \nabla w & \nabla w \times \nabla u & \nabla u \times \nabla v \\ | & | & | \\ | & | & | \end{pmatrix}$$

For ∇u , we have

$$(5.10) \quad \nabla \cdot A \nabla u = \nabla \cdot (\nabla v \times \nabla w) = \nabla w \cdot (\nabla \times \nabla v) - \nabla v \cdot (\nabla \times \nabla w) = 0$$

since $\nabla \times \nabla$ results in zero vector. This also holds for ∇v and ∇w .

Therefore, we compute divergence on both sides of Equation 5.7 to get the following equations

$$(5.11) \quad \begin{aligned} \nabla \cdot A \nabla u &= 0 \\ \nabla \cdot A \nabla v &= 0 \\ \nabla \cdot A \nabla w &= 0 \end{aligned}$$

Furthermore, we define $\nabla \cdot A \nabla$ as the 3D generalized Laplacian operator.

5.1.3. Discretisation and implementation. In the 2D case, we typically triangularize the domain to obtain finite elements and then define a piecewise linear function on that domain to approximate the smooth map. In the 3D case, we need to define the piecewise linear function on tetrahedrons serving as the elements.

Consider a 3D simply connected domain Ω discretized into a tetrahedral mesh containing vertices and tetrahedrons, each of which includes four vertices. Also, the order of the vertices in a tetrahedron $T = [v_i, v_j, v_k, v_l]$ should satisfy a condition: the determinant of the matrix consisting of the three vectors $v_j - v_i$, $v_k - v_i$, and $v_l - v_i$ must be positive.

We denote the piecewise linear map used to approximate f as \tilde{f} , which satisfies $\tilde{f}(v) = f(v)$, where v is the vertex of the tetrahedral mesh. To compute the 3D quasiconformal representation for \tilde{f} , we need to compute the 3D quasiconformal representation at each point in Ω . However, since \tilde{f} is piecewise linear, the Jacobian matrices $D_{\tilde{f}}$ at each point in a tetrahedron T are equal to each other, resulting in the same polar decomposition and 3D quasiconformal representation. Therefore, we simply need to approximate the Jacobian matrices at each tetrahedron T , denoted as $D_{\tilde{f}}(T)$. The restriction of \tilde{f} on each tetrahedron T can be written as

$$(5.12) \quad \tilde{f}|_T(x, y, z) = \begin{pmatrix} \alpha_T x + \beta_T y + \gamma_T z + \delta_T \\ \epsilon_T x + \zeta_T y + \eta_T z + \iota_T \\ \kappa_T x + \lambda_T y + \xi_T z + \rho_T \end{pmatrix}$$

Hence the Jacobian matrix for \tilde{f} on T is

$$(5.13) \quad D_{\tilde{f}}(T) = \begin{pmatrix} \alpha_T & \beta_T & \gamma_T \\ \epsilon_T & \zeta_T & \eta_T \\ \kappa_T & \lambda_T & \xi_T \end{pmatrix}$$

Then we compute the polar decomposition to $D_{\tilde{f}}(T)$ as 5.1 to get the a, b and c and \tilde{W} from which θ_x, θ_y and θ_z can be calculated. With this information, we can get the 3D quasiconformal representation for the tetrahedron T .

To reconstruct the mapping \tilde{f} , we can either use Equation 5.2 and θ_x, θ_y and θ_z to reconstruct W or use the W in the above computation directly. The matrix A can be computed according to Equation 5.8.

To obtain the discretized version of Equation 5.11, we should first derive $D_{\tilde{f}}(T)$. Suppose a tetrahedron $T = [v_i, v_j, v_k, v_l]$ consists of four vertices v_i, v_j, v_k and v_l . Let $w_I = f(v_I)$, $v_I = (k_I, l_I, m_I)$ and $w_I = (n_I, o_I, p_I)$, where $I = i, j, k, l$. Then we have the equation

$$(5.14) \quad D_{\tilde{f}}(T)X = Y$$

where

$$(5.15) \quad X = \begin{pmatrix} k_j - k_i & k_k - k_i & k_l - k_i \\ l_j - l_i & l_k - l_i & l_l - l_i \\ m_j - m_i & m_k - m_i & m_l - m_i \end{pmatrix} \text{ and } Y = \begin{pmatrix} n_j - n_i & n_k - n_i & n_l - n_i \\ o_j - o_i & o_k - o_i & o_l - o_i \\ p_j - p_i & p_k - p_i & p_l - p_i \end{pmatrix}$$

Then moving the matrix X to the right, we have

$$(5.16) \quad D_{\tilde{f}}(T) = YX^{-1}$$

For simplicity, we index the values in X^{-1} by the form x_{ij} , where i and j are the row and column of the indexed entry.

We define

$$(5.17) \quad \begin{aligned} A_T^i &= -(x_{11} + x_{21} + x_{31}), & A_T^j &= x_{11}, & A_T^k &= x_{21} \text{ and } A_T^l = x_{31} \\ B_T^i &= -(x_{12} + x_{22} + x_{32}), & B_T^j &= x_{12}, & B_T^k &= x_{22} \text{ and } B_T^l = x_{32} \\ C_T^i &= -(x_{13} + x_{23} + x_{33}), & C_T^j &= x_{13}, & C_T^k &= x_{23} \text{ and } C_T^l = x_{33} \end{aligned}$$

Then we have the following result.

$$(5.18) \quad D_{\tilde{f}}(T) = \begin{pmatrix} A_T^i n_i + A_T^j n_j + A_T^k n_k + A_T^l n_l & B_T^i n_i + B_T^j n_j + B_T^k n_k + B_T^l n_l & C_T^i n_i + C_T^j n_j + C_T^k n_k + C_T^l n_l \\ A_T^i o_i + A_T^j o_j + A_T^k o_k + A_T^l o_l & B_T^i o_i + B_T^j o_j + B_T^k o_k + B_T^l o_l & C_T^i o_i + C_T^j o_j + C_T^k o_k + C_T^l o_l \\ A_T^i p_i + A_T^j p_j + A_T^k p_k + A_T^l p_l & B_T^i p_i + B_T^j p_j + B_T^k p_k + B_T^l p_l & C_T^i p_i + C_T^j p_j + C_T^k p_k + C_T^l p_l \end{pmatrix}$$

Then the divergence operator is defined as a vector $(A_T^i, B_T^i, C_T^i)^T$. Denoting the three row vectors of $D_{\tilde{f}}(T)$ as $\nabla u, \nabla v$ and ∇w , then by Equation 5.11, we have the following three values for tetrahedron T at vertex v_i .

$$(5.19) \quad \begin{aligned} div_n &= (A_T^i, B_T^i, C_T^i)^T \cdot A \nabla u \\ div_o &= (A_T^i, B_T^i, C_T^i)^T \cdot A \nabla v \\ div_p &= (A_T^i, B_T^i, C_T^i)^T \cdot A \nabla w \end{aligned}$$

Let $\mathcal{N}(v_i)$ denote the set containing the incident tetrahedrons of v_i , then we can write the following equation to get the discrete approximation for Equation 5.11 at each vertex of the mesh.

$$(5.20) \quad \begin{aligned} \sum_{T \in \mathcal{N}(v_i)} Vol(T) \cdot div_n &= 0 \\ \sum_{T \in \mathcal{N}(v_i)} Vol(T) \cdot div_o &= 0 \\ \sum_{T \in \mathcal{N}(v_i)} Vol(T) \cdot div_p &= 0 \end{aligned}$$

where $Vol(T)$ denotes the volume of T . Note that the unknowns in $w_I = (n_I, o_I, p_I)$ representing the resulting mapping have been introduced in the matrix Y , and by Equation 5.16, $D_{\tilde{f}}(T)$ contains the unknowns. As a result, in Equation 5.19, vectors $\nabla u, \nabla v$ and ∇w contain the

unknowns. Also, we observe that the parameters in $\nabla u, \nabla v$ and ∇w are the same, implying that the three equations in Equation 5.19 are the same except the unknowns. Consequently, in practice, it is only necessary to construct one of the three equations. By reorganizing the equation and introducing boundary conditions, three linear systems of size $N^3 \times N^3$ can be formed, from which the mapping \tilde{f} can be reconstructed.

5.2. Representation for Mapping with Foldings and Folding Removal. One of the most important features of LBS is to eliminate foldings from 2D mappings. In this section, we extend the above representation to describe mappings with foldings and propose a simple but effective algorithm to eliminate foldings from these mappings.

5.2.1. Representation. In the previous sections, we have introduced the 3D quasiconformal solver to describe and reconstruct bijective maps. To achieve our ultimate goal of eliminating the foldings from the map, we need to first extend the aforementioned 3D quasiconformal representation for diffeomorphism to mappings with foldings. With this extension, we can propose an algorithm to eliminate their foldings easily.

Suppose f has reverse orientation in domain $X^- \in X$, and for any point $p \in X^-$, we have $\det(D_f(\tilde{p})) \leq 0$. Note that Equation 5.1 still holds for folded maps, since it is valid for any matrix. When $\det(D_f(p)) < 0$, p does not lie on the folding line. In this case, from Equation 5.1, we know that the matrix P must be positive definite, which implies $\det(U) = -1$. Let $L = QDQ^T$, where Q is an orthogonal matrix and D is a diagonal matrix where k of the diagonal elements are -1 and the remaining elements are 1. Here, k is an odd number in the set $\{1, 3\}$, so that $\det(D) = -1$, and $\det(L) = \det(L^{-1}) = -1$. We notice that $UL^{-1} = UQD^{-1}Q^T = UQDQ^T$ is an orthogonal matrix, the determinant of which is 1, meaning that it is a rotation matrix. Let $\tilde{U} = U(p)L^{-1}$, and $\tilde{P} = LP(p)$, then $\det(\tilde{U}) = 1$ and we have

$$D_f(p) = U(p)P(p) = U(p)L^{-1}LP(p) = \tilde{U}\tilde{P}$$

$$\text{Thus } \det(D_f(p)) = \det(\tilde{U})\det(\tilde{P}) = \det(\tilde{U})\det(L)\det(P) = -\sqrt{D_f(p)^T D_f(p)} = -abc.$$

Since the matrix L can be randomly selected based on the above conditions, we can choose a matrix that has the same eigenvectors as P , i.e., $Q = W$, and has eigenvalues 1, 1 and -1 , regardless of their order. Let $\tilde{\Sigma} = D\Sigma$, then

$$(5.21) \quad \tilde{P} = LP(p) = WDW^T W\Sigma W^T = WD\Sigma W^T = W\tilde{\Sigma}W^T$$

Therefore, we get \tilde{P} simply by reversing the sign of one of the eigenvalues of the matrix P . The question then becomes which eigenvalue's sign should be flipped.

We would like to show that the dilation parts caused by flipping the sign of one of the three eigenvalues of P , and by flipping all of them, are equivalent up to rotation. To see this, let D_1 and D_2 are the matrices with diagonal elements $(-1, -1, -1)$ and $(1, 1, -1)$ respectively. By the above conclusion, we know that there exist two rotation matrices \tilde{U}_1 and \tilde{U}_2 such that

$$(5.22) \quad D_f(p) = \tilde{U}_1 \underbrace{WD_1\Sigma W^T}_{\tilde{P}_1} = \tilde{U}_2 \underbrace{WD_2\Sigma W^T}_{\tilde{P}_2}$$

Thus we have $\tilde{P}_1 = \tilde{U}_1^{-1}\tilde{U}_2\tilde{P}_2$. Since \tilde{U}_1 and \tilde{U}_2 are rotation matrices, $\tilde{U}_1^{-1}\tilde{U}_2$ is also a rotation matrix. So we conclude that \tilde{P}_1 and \tilde{P}_2 are equivalent dilation up to a rotation. This

conclusion also holds when D_2 has diagonal elements $(-1, 1, 1)$ or $(1, -1, 1)$. So the dilation parts in these four cases are equivalent to each other up to rotation. Since the mappings caused by rotation are conformal, we can omit them when discussing quasiconformal representation and only pay attention to the dilation part.

In the 2D case, the eigenvalues of the dilation part of the mapping at a specific point are given by $1 - |\mu|$ and $1 + |\mu|$, and $1 + |\mu| \geq |1 - |\mu|| \geq 0$. When $\|\mu\|_\infty > 1$, the mapping contains foldings, as the eigenvalue $1 - |\mu|$ becomes negative at some points. Analogous to the 2D case, in the 3D case, we choose to reverse the sign of the smallest eigenvalue of P , i.e., c in Σ .

In summary, we extend the 3D quasiconformal representation to the case $D_f(p) < 0$ by the following form

$$(5.23) \quad D_f(p) = \tilde{U}\tilde{P} = \tilde{U}W D \Sigma W^T$$

where $W \Sigma W^T$ is the eigenvalue decomposition of $\sqrt{D_f(p)^T D_f(p)}$, and D is a matrix with diagonal elements $(1, 1, -1)$. \tilde{U} is a rotation matrix unrelated to local dilation. By adjusting the direction of the column vectors in the matrix W , and converting this matrix to Euler angles as we have done in the last section, we obtain a representation that can describe the local dilation when $D_f(p) < 0$.

5.2.2. Folding removal. In numerous applications, such as medical image registration and segmentation, the existence of folding contradicts our prior knowledge. Unfortunately, conventional registration methods often produce mappings that exhibit folding. In the context of 2D scenarios, various algorithms have been proposed to eliminate these foldings. Among them, algorithms based on quasiconformal geometry have achieved significant success in preserving orientation. These quasiconformal algorithms primarily rely on controlling the magnitude of Beltrami coefficients. This control is achieved through approaches such as minimizing energy functionals associated with Beltrami coefficients or truncating their magnitudes and solving PDEs to obtain a fixed mapping. In the case of 3D scenarios, a similar attempt has been made by [34], where they introduced a distortion measure that allows for controlling its magnitude to suppress foldings. In this paper, we will present an effective algorithm for removing foldings from mappings, which shares similarities with the quasiconformal method employed in 2D.

In the 2D case, truncating the magnitude of μ such that $\|\mu\|_\infty < 1$ and reconstructing the mapping eliminates foldings. Sometimes a small number of foldings may still exist due to the boundary condition, and we can repeat the procedure until all foldings are eliminated. Truncating the magnitude of μ is equivalent to setting both eigenvalues $1 - |\mu|$ and $1 + |\mu|$ to positive values. Also, when $\|\mu\|_\infty < 1$, the ratio of the large dilation and the small dilation

$$K = \frac{1 + |\mu|}{1 - |\mu|}$$

is under control.

Similarly, in the 3D case, we can reverse the sign of the negative diagonal element of $\tilde{\Sigma} = D \Sigma$ to obtain c . However, the ratio of the largest dilation a and the smallest dilation c is not under control if we only make the negative diagonal element of $\tilde{\Sigma}$ positive. Thus we propose a method to cope with this problem.

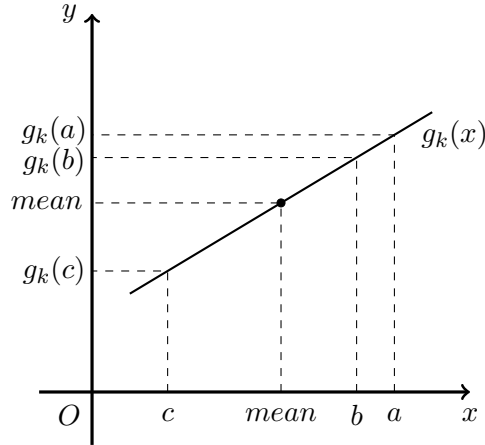


Figure 2: Illustration for the function $g_k(x)$, which passes through the point $(mean, mean)$ with slope k depending on $K_{threshold}$. With suitable k , $g_k(x)$ maps a and c to $g_k(a)$ and $g_k(c)$ such that $g_k(a)/g_k(c) = K_{threshold}$.

In the following, we use notations a, b and c to denote the resulting positive values after the step of reversing the sign of negative eigenvalues. By the convention mentioned above in the eigenvalue decomposition, we have $a \geq b \geq c > 0$. And we define the ratio of the largest and smallest dilation K as

$$K(a, b, c) = \frac{\max(a, b, c)}{\min(a, b, c)} = \frac{a}{c} \geq 1$$

Our goal is to control $K(a, b, c)$ for each tetrahedron such that it does not exceed the threshold $K_{threshold}$ set by the user.

We compute the mean of the maximal and minimal dilation

$$mean = \frac{a + c}{2}$$

When $K(a, b, c) > K_{threshold}$ for some tetrahedrons, we can use the following one variable function $g_k(x)$ to map the three eigenvalues to their new values such that $K(g_k(a), g_k(b), g_k(c)) = K_{threshold}$, and when $K(a, b, c) \leq K_{threshold}$, we keep a, b and c without change. The graph for $g_k(x)$ is shown in Figure 2.

$$g_k(x) = k(x - mean) + mean$$

Then the question becomes how to determine the slope k in $g_k(x)$. when $K(a, b, c) > K_{threshold}$, let

$$(5.24) \quad \frac{g_k(\max(a, b, c))}{g_k(\min(a, b, c))} = \frac{g_k(a)}{g_k(c)} = K_{threshold}$$

By simple derivation, we obtain

$$(5.25) \quad k = \frac{(K_{threshold} - 1)mean}{(K_{threshold} + 1)(a - mean)}$$

Apart from the above constraint, we also require that $g_k(a) \geq g_k(c) > 0$. And we notice that this condition is automatically satisfied if $K_{threshold} \geq 1$. To see this, we shall first check $g_k(a) \geq g_k(c)$, and then check $g_k(c) > 0$.

- When $K(a, b, c) > K_{threshold} \geq 1$, we have $a > c$, $(K_{threshold} - 1) \geq 0$ and $(K_{threshold} + 1) \geq 2 > 0$. Since $a > c > 0$, we have $mean = \frac{a+c}{2} > 0$ and $a - mean = a - \frac{a+c}{2} = \frac{a-c}{2} > 0$. Therefore, $k \geq 0$, indicating that $g_k(x)$ is a monotone increasing or a constant function. By $a > c$, we have $g_k(a) \geq g_k(c)$.
- Also, $0 \leq \frac{K_{threshold}-1}{K_{threshold}+1} < 1$, meaning that $k < \frac{mean}{a-mean} = \frac{-mean}{c-mean}$. Thus $g_k(c) = k(c - mean) + mean > -mean + mean = 0$.

Therefore, the total algorithm is as the following: we first set the $K_{threshold} \geq 1$. For each tetrahedron, we compute its $K(a, b, c)$. If $K(a, b, c) > K_{threshold}$, then we compute the k according to Equation 5.25 for the function $g_k(x)$, and then assign $g_k(a)$, $g_k(b)$ and $g_k(c)$ to a , b and c respectively.

Note that although we show that $K_{threshold}$ can be close to 1, we prefer to assign it a large number in order to preserve the distortion information of the mappings. In the following experiments, we let $K_{threshold} = 10$.

After the above adjustment, all the diagonal elements of $\tilde{\Sigma}$ become positive, i.e., a , b and c , and $K(a, b, c)$ is under control. We then use the same procedure as in the diffeomorphism case to reconstruct the mapping. We will show some experimental results below to demonstrate the effectiveness of this method.

5.3. Pseudo-codes. This section provides a summary of the algorithms discussed in the previous sections by presenting the pseudo-codes for each method, as shown in Algorithm 5.1, 5.2 and 5.3.

Note that in Algorithm 5.2, we add an option *CORRECT_DIRECTION*. When it is set to *True*, the algorithm adjusts the dilation and reconstructs the mapping as mentioned above. Interestingly, when we set it to *False*, the algorithm uses the representation for the two cases to reconstruct the mappings with folding directly, and the experimental results show that it can reconstruct them perfectly, as shown in the next section.

6. Experiments. This section presents experimental results demonstrating the effectiveness of our proposed 3D quasiconformal representation and solver on 3D tetrahedral meshes. For simplicity, we implement our experiments on a cubic domain with $20 \times 20 \times 20$ vertices. This cube can be considered as composed of $19 \times 19 \times 19$ unit cubes.

The first thing to do is to discretize the domain with the vertices. We notice that each cube can be decomposed into 5 tetrahedrons. Also, the methods to decompose odd and even cubes should be different, as shown in Figure 3.

For the following experiments, we use the same boundary condition as follows

- f maps vertices in the plane $\{(0, y, z) \in \mathbb{R}^3\}$ to the plane $\{(0, y, z) \in \mathbb{R}^3\}$.
- f maps vertices in the plane $\{(1, y, z) \in \mathbb{R}^3\}$ to the plane $\{(1, y, z) \in \mathbb{R}^3\}$.
- f maps vertices in the plane $\{(x, 0, z) \in \mathbb{R}^3\}$ to the plane $\{(x, 0, z) \in \mathbb{R}^3\}$.

Algorithm 5.1 3D quasiconformal representation computation for 3D mapping

Input: $V_s = \{v_{s_1}, v_{s_2}, \dots, v_{s_n}\}$ and $V_t = \{v_{t_1}, v_{t_2}, \dots, v_{t_n}\}$, where n is the number of vertices in the mesh; $F = \{(i_1, i_2, i_3, i_4), (j_1, j_2, j_3, j_4), \dots\}$, where (i_1, i_2, i_3, i_4) represents a tetrahedron with vertices in V_s and V_t indexed by i_1, i_2, i_3 and i_4 .

Output: 3D quasiconformal representation $\mu(T)$ for $T \in F$

for $T \in F$ **do**

 Compute the Jacobian matrix $D_f(T)$ with V_s, V_t and F

$P \leftarrow D_f(T)^T D_f(T)$

 Compute eigenvalue decomposition: $P = W D W^T$

$\Sigma \leftarrow \sqrt{D}$

$a, b, c \leftarrow \Sigma_{11}, \Sigma_{22}, \Sigma_{33}$

\triangleright By convention, we assume $a \geq b \geq c$.

if $\det(D_f(T)) < 1$ **then**

$c \leftarrow -c$

end if

if $\det(W) = -1$ **then**

 Update W by multiplying the first column by -1 .

end if

$\theta_x \leftarrow \text{atan2}(r_{32}, r_{33})$

$\triangleright r_{ij}$ denotes the entry in the i row j column of W

$\theta_y \leftarrow \text{atan2}(-r_{31}, \sqrt{r_{32}^2 + r_{33}^2})$

$\theta_z \leftarrow \text{atan2}(r_{21}, r_{11})$

$\mu(T) \leftarrow (a, b, c, \theta_x, \theta_y, \theta_z)$

end for

- f maps vertices in the plane $\{(x, 1, z) \in \mathbb{R}^3\}$ to the plane $\{(x, 1, z) \in \mathbb{R}^3\}$.
- f maps vertices in the plane $\{(x, y, 0) \in \mathbb{R}^3\}$ to the plane $\{(x, y, 0) \in \mathbb{R}^3\}$.
- f maps vertices in the plane $\{(x, y, 1) \in \mathbb{R}^3\}$ to the plane $\{(x, y, 1) \in \mathbb{R}^3\}$.

6.1. Mesh reconstruction. In this section, we would like to show some results of reconstruction. First, we randomly generate meshes to form bijective mappings. We then compute their 3D quasiconformal representations and reconstruct them based on these representations and the boundary conditions. Finally, we calculate the L^2 norm between the original mappings and the reconstructed mappings to determine the reconstruction error.

Figures 4 and 5 show the reconstruction results for two bijective mappings, and the reconstruction errors are $1.4596e-12$ and $1.4765e-12$, respectively. These small errors demonstrate that our approach is effective at reconstructing mappings using their 3D quasiconformal representations, yielding precise results for bijective mappings.

6.2. Folding Removal. In this section, we would like to show some experiments to eliminate foldings from non-bijective mappings. Given two mappings with 16,919 and 2,579 folded tetrahedrons, we use our solver to modify the tetrahedral meshes iteratively. At each iteration, in order to address the folds, we reverse negative eigenvalues to positive values and adjust them to control the distortion. Experimental results are shown in Figures 6 and 7.

Algorithm 5.2 Mapping reconstruction from 3D quasiconformal representation

Input: $V_s = \{v_{s_1}, v_{s_2}, \dots, v_{s_n}\}$, where n is the number of vertices in the mesh; $F = \{(i_1, i_2, i_3, i_4), (j_1, j_2, j_3, j_4), \dots\}$, where (i_1, i_2, i_3, i_4) represents a tetrahedron with vertices in V_s indexed by i_1, i_2, i_3 and i_4 . $\mu(T) = (a(T), b(T), c(T), \theta_x(T), \theta_y(T), \theta_z(T))$ for $T \in F$. A boolean variable “CORRECT_DIRECTION” indicating if folding elimination will be performed. $K_{threshold}$ should be provided if “CORRECT_DIRECTION” is True.

Output: V_t

for $T \in F$ **do**

$W \leftarrow R(\theta_x(T), \theta_y(T), \theta_z(T))$ \triangleright R is the 3D rotation matrix with Euler angles

if CORRECT_DIRECTION is True **then**

$a(T), b(T), c(T) \leftarrow \text{adjust_eigval}(a(T), b(T), c(T), K_{threshold})$ \triangleright Algorithm 5.3

end if

Compute A by Equation 5.8 with $a(T), b(T), c(T)$ and W

for $v \in T$ **do**

$\tilde{T} \leftarrow$ reorganized T \triangleright To ensure the correctness of chirality.

Construct X

Compute X^{-1}

Compute $A_{\tilde{T}}^i, B_{\tilde{T}}^i, C_{\tilde{T}}^i, A_{\tilde{T}}^j, B_{\tilde{T}}^j, C_{\tilde{T}}^j, A_{\tilde{T}}^k, B_{\tilde{T}}^k, C_{\tilde{T}}^k, A_{\tilde{T}}^l, B_{\tilde{T}}^l, C_{\tilde{T}}^l$ to construct ∇u .

$\text{div}_n(v, T) \leftarrow (A_{\tilde{T}}^i, B_{\tilde{T}}^i, C_{\tilde{T}}^i)^T \cdot A \nabla u$

$\text{Div}_{vT} \leftarrow \text{Vol}(T) \cdot \text{div}_n(v, T)$

end for

end for

Create an $N^3 \times N^3$ matrix \mathcal{C}

for $v \in V_s$ **do**

Fill in the matrix \mathcal{C} according to $\sum_{T \in \mathcal{N}(v)} \text{Div}_{vT} = 0$

end for

Introduce the boundary condition to construct an $N^3 \times N^3$ linear system with \mathcal{C} .

Solve the system to obtain V_t

Algorithm 5.3 adjust_eigval

Input: $a(T)$, $b(T)$ and $c(T)$ for each T in the tetrahedral mesh F , $a(T) \geq b(T) \geq |c(T)|$; a constant $K_{threshold} \geq 1$.

Output: Processed $a(T)$, $b(T)$ and $c(T)$.

for $T \in F$ **do**

$c(T) \leftarrow |c(T)|$

$K = \frac{a(T)}{c(T)}$

if $K > K_{threshold}$ **then**

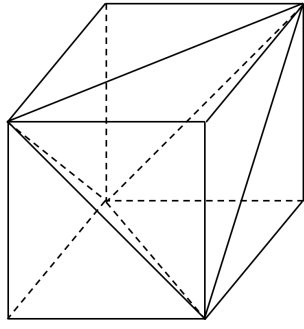
$mean = \frac{a(T) + c(T)}{2}$

$k = \frac{(K_{threshold} - 1)mean}{(K_{threshold} + 1)(a(T) - mean)}$

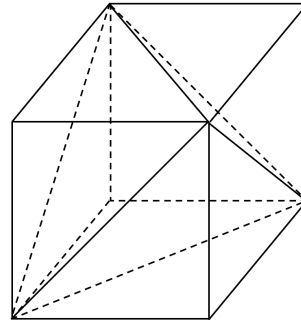
$a(T), b(T), c(T) \leftarrow g_k(a(T)), g_k(b(T)), g_k(c(T))$ $\triangleright g_k(x) = k(x - mean) + mean$

end if

end for

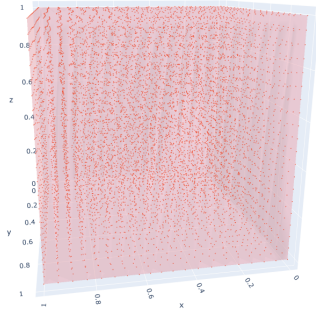


(a) Decomposition method for odd cubes

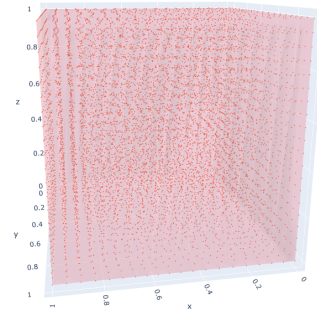


(b) Decomposition method for even cubes

Figure 3: Illustration for decomposition methods



(a) The original tetrahedral mesh without folding.



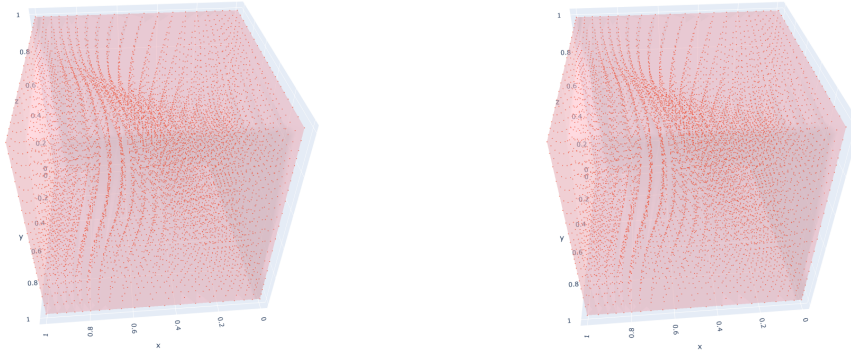
(b) The reconstructed tetrahedral mesh.

Figure 4: Mesh reconstruction result of mapping without folding. The reconstruction error is $1.4596e-12$.

The experiments show that our solver is able to completely remove foldings from the given mappings, successfully ensuring bijectivity.

In the first mapping, a total of 16,919 folded tetrahedrons were observed (refer to Figure 6a for visual representation). This case was considered extreme due to the large number of folded tetrahedrons present. The black regions in Figure 6b indicate the locations of the folded tetrahedrons. Surprisingly, when the elliptic PDE was constructed and solved without any adjustments to its 3D representation, the original mapping could be accurately reconstructed, as demonstrated in Figure 6c. By modifying the 3D representation and employing the algorithm, the solver successfully eliminated all folds within three iterations. This significant improvement is evident in Figure 6d, where no folded tetrahedrons remain.

In the second mapping, a smaller number of folded tetrahedrons, specifically 2,579, were identified (refer to Figure 7a). Compared to the previous case, this mapping exhibited a



(a) The original tetrahedral mesh without folding. (b) The reconstructed tetrahedral mesh.

Figure 5: Mesh reconstruction result of mapping without folding. The reconstruction error is $1.4765e-12$.

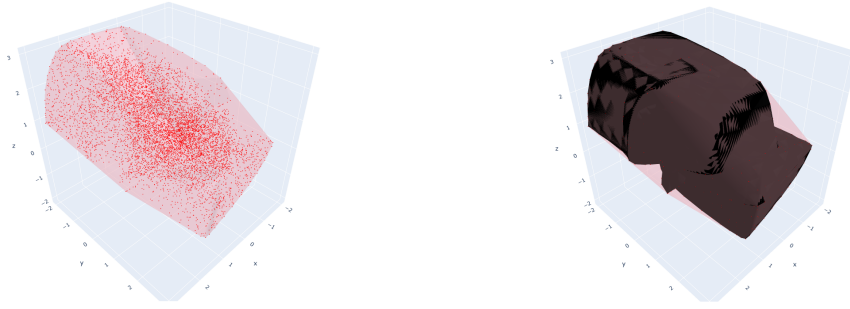
significantly lower incidence of folded tetrahedrons. Figure 7b highlights the black regions representing the folded tetrahedrons. Interestingly, when the elliptic PDE was constructed and solved without any adjustments to its 3D representation, the original mapping could still be precisely reconstructed, as shown in Figure 7c. However, what is truly remarkable is that the solver was able to eliminate all folds after just one iteration, as depicted in Figure 7d.

The experiments conducted provide compelling evidence that our approach is highly effective in eliminating folds from non-bijective mappings. By adjusting eigenvalues, constructing and solving the PDE, our solver is capable of efficiently removing folds in just a few steps, ultimately making the mappings bijective. These results underscore the robustness and effectiveness of our algorithm in addressing the challenge of fold elimination. Thus, we successfully extend the folding removal method based on Beltrami coefficients from 2D space to 3D, significantly broadening its scope and utility. This generalization further enhances the applicability of our algorithm across a wide range of practical scenarios, paving the way for its integration into various fields where non-bijective mappings are encountered.

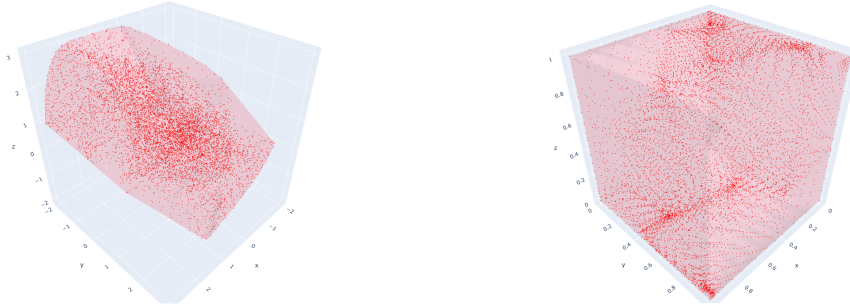
6.3. Mesh generation. In this section, we would like to show some results in which we assign a 3D quasiconformal representation to a tetrahedral mesh and utilize it to generate a mesh that aligns with our expectations.

In the experiment, we split the tetrahedral mesh along the y -axis midpoint. We want the left half, with y -coordinates closer to 0, to contract while the right half expands. We control this by assigning different 3D quasiconformal representations to the two halves. In the first experiment, we assign $(1, 0.5, 1, 0, 0, 0)$ to the left half and $(1, 1, 1, 0, 0, 0)$ to the right half. In the second experiment, we assign $(1, 0.1, 1, 0, 0, 0)$ to the left half and $(1, 2, 1, 0, 0, 0)$ to the right half.

As shown in Figure 8, the results meet our imagination. The 3D quasiconformal representation we designed adjusts one parameter related to the y component controlling the



(a) The original tetrahedral mesh with 16,919 folded tetrahedrons. (b) The original tetrahedral mesh with 16,919 folded tetrahedrons, shown in black.



(c) The reconstructed tetrahedral mesh. The reconstruction error is $1.9963e-6$. (d) The processed tetrahedral mesh without folding.

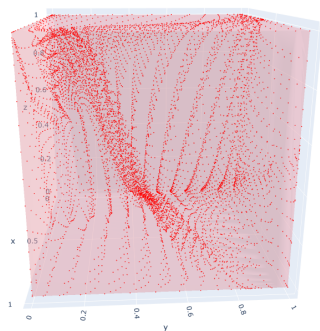
Figure 6: Folding removal result of mapping with 16,919 folded tetrahedrons.

amount of contraction and expansion along the y-axis. Decreasing this parameter contributes to contracting the mesh along the y-axis while increasing it leads to expansion.

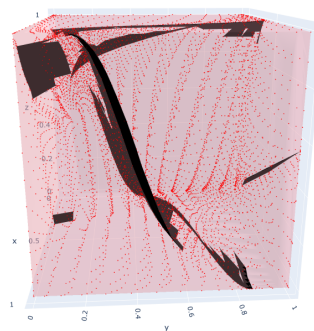
In conclusion, designing a 3D quasiconformal representation enabled us to generate meshes that exhibit the non-uniform scaling required to match our intended designs for contracted and expanded domains. With further refinements, this technique has potential for generating high-quality meshes in applications that require distorted or non-uniform representations of 3D shapes.

7. Conclusion. In this paper, we have proposed an effective 3D quasiconformal representation to describe the local dilation of 3D mappings. This representation, along with the associated solver similar to Linear Beltrami Solver, allows us to generalize the distortion control capabilities previously only possible in 2D space to 3D space.

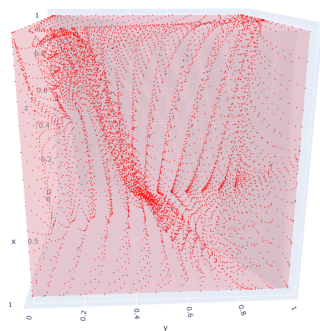
We demonstrated the effectiveness of our proposed 3D quasiconformal representation and solver in several ways. First, by reconstructing randomly generated tetrahedral meshes with high precision, proving that the representation can encode the distortion of 3D mappings. Second, by eliminating foldings from non-bijective mappings through iterative improvement, showing that our algorithm can be used to remove foldings from mappings. And third, by



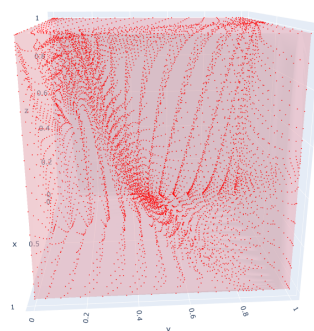
(a) The original tetrahedral mesh with 2,579 folded tetrahedrons.



(b) The original tetrahedral mesh with 2,579 folded tetrahedrons, shown in black.



(c) The reconstructed tetrahedral mesh. The reconstruction error is $1.9601e-8$.



(d) The processed tetrahedral mesh without folding.

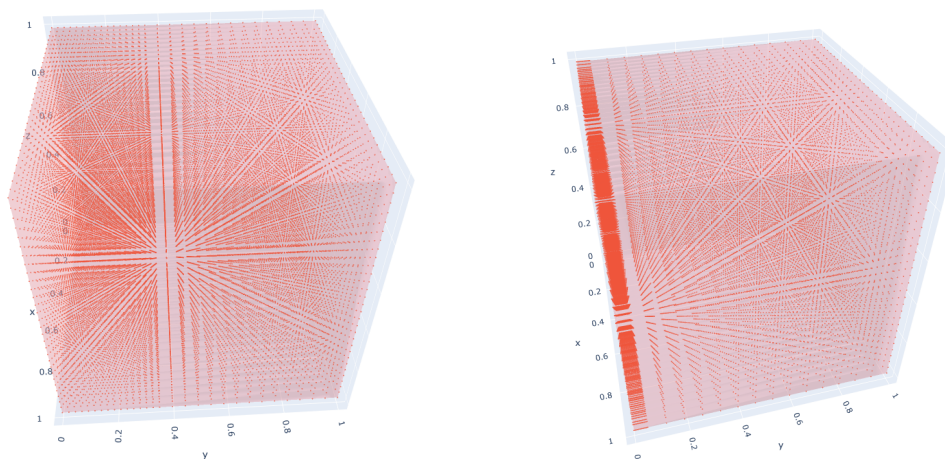
Figure 7: Folding removal result of mapping with 2,579 folded tetrahedrons.

generating tetrahedral meshes that exhibit the non-uniform scaling required to match our intended designs.

The ability to analyze and control distortion in 3D space opens up new possibilities in various fields. For applications processing or analyzing 3D data, handling distortions in an efficient and quantitative manner will enable more robust and reliable results.

In future work, we plan to improve the computational efficiency of our algorithm and extend it to handle more complex deformations. We also aim to explore more applications where our technique could prove useful, including 3D image registration and image segmentation.

In summary, we have introduced an effective tool that, for the first time, fills the gap of describing and manipulating distortions in 3D space. The potential applications of our work are far-reaching, and we hope this newfound capability will prove invaluable for research involving 3D shapes and information.



(a) The 3D quasiconformal representation of the left part is $(1, 0.5, 1, 0, 0, 0)$, while that of the right part is $(1, 1, 1, 0, 0, 0)$.
 (b) The 3D quasiconformal representation of the left part is $(1, 0.1, 1, 0, 0, 0)$, while that of the right part is $(1, 2, 1, 0, 0, 0)$.

Figure 8: Results of mesh generation.

REFERENCES

- [1] H. L. CHAN, H. LI, AND L. M. LUI, *Quasi-conformal statistical shape analysis of hippocampal surfaces for alzheimer's disease analysis*, Neurocomputing, 175 (2016), pp. 177–187, <https://doi.org/https://doi.org/10.1016/j.neucom.2015.10.047>, <https://www.sciencedirect.com/science/article/pii/S0925231215015064>.
- [2] H.-L. CHAN, S. YAN, L.-M. LUI, AND X.-C. TAI, *Topology-preserving image segmentation by beltrami representation of shapes*, Journal of Mathematical Imaging and Vision, 60 (2018), pp. 401–421.
- [3] H.-L. CHAN, H.-M. YUEN, C.-T. AU, K. C.-C. CHAN, A. M. LI, AND L.-M. LUI, *Quasi-conformal geometry based local deformation analysis of lateral cephalogram for childhood osa classification*, arXiv preprint arXiv:2006.11408, (2020).
- [4] K. CHEN, L. M. LUI, AND J. MODERSITZKI, *Image and surface registration*, in Handbook of Numerical Analysis, vol. 20, Elsevier, 2019, pp. 579–611.
- [5] Q. CHEN, Z. LI, AND L. M. LUI, *A deep learning framework for diffeomorphic mapping problems via quasi-conformal geometry applied to imaging*, arXiv preprint arXiv:2110.10580, (2021).
- [6] G. P. CHOI, H. L. CHAN, R. YONG, S. RANJITKAR, A. BROOK, G. TOWNSEND, K. CHEN, AND L. M. LUI, *Tooth morphometry using quasi-conformal theory*, Pattern Recognition, 99 (2020), p. 107064.
- [7] G. P. CHOI, D. QIU, AND L. M. LUI, *Shape analysis via inconsistent surface registration*, Proceedings of the Royal Society A, 476 (2020), p. 20200147.
- [8] P. T. CHOI, K. C. LAM, AND L. M. LUI, *Flash: Fast landmark aligned spherical harmonic parameterization for genus-0 closed brain surfaces*, SIAM Journal on Imaging Sciences, 8 (2015), pp. 67–94.
- [9] P. T. CHOI AND L. M. LUI, *Fast disk conformal parameterization of simply-connected open surfaces*, Journal of Scientific Computing, 65 (2015), pp. 1065–1090.
- [10] M. DESBRUN, M. MEYER, AND P. ALLIEZ, *Intrinsic parameterizations of surface meshes*, in Computer graphics forum, vol. 21, Wiley Online Library, 2002, pp. 209–218.
- [11] X. GU, Y. WANG, T. F. CHAN, P. M. THOMPSON, AND S.-T. YAU, *Genus zero surface conformal mapping and its application to brain surface mapping*, IEEE transactions on medical imaging, 23 (2004), pp. 949–958.

- [12] Y. GUO, Q. CHEN, G. P. CHOI, AND L. M. LUI, *Automatic landmark detection and registration of brain cortical surfaces via quasi-conformal geometry and convolutional neural networks*, *Computers in Biology and Medicine*, (2023), p. 107185.
- [13] K. C. LAM, X. GU, AND L. M. LUI, *Genus-one surface registration via teichmüller extremal mapping*, in *International Conference on Medical Image Computing and Computer-Assisted Intervention*, Springer, 2014, pp. 25–32.
- [14] K. C. LAM, X. GU, AND L. M. LUI, *Landmark constrained genus-one surface teichmüller map applied to surface registration in medical imaging*, *Medical image analysis*, 25 (2015), pp. 45–55.
- [15] K. C. LAM AND L. M. LUI, *Landmark-and intensity-based registration with large deformations via quasi-conformal maps*, *SIAM Journal on Imaging Sciences*, 7 (2014), pp. 2364–2392.
- [16] K. C. LAM AND L. M. LUI, *Quasi-conformal hybrid multi-modality image registration and its application to medical image fusion*, in *International Symposium on Visual Computing*, Springer, 2015, pp. 809–818.
- [17] B. LÉVY, S. PETITJEAN, N. RAY, AND J. MAILLOT, *Least squares conformal maps for automatic texture atlas generation*, *ACM transactions on graphics (TOG)*, 21 (2002), pp. 362–371.
- [18] L. M. LUI, K. C. LAM, T. W. WONG, AND X. GU, *Texture map and video compression using beltrami representation*, *SIAM Journal on Imaging Sciences*, 6 (2013), pp. 1880–1902.
- [19] L. M. LUI, K. C. LAM, S.-T. YAU, AND X. GU, *Teichmüller mapping (t-map) and its applications to landmark matching registration*, *SIAM Journal on Imaging Sciences*, 7 (2014), pp. 391–426.
- [20] L. M. LUI AND C. WEN, *Geometric registration of high-genus surfaces*, *SIAM Journal on Imaging Sciences*, 7 (2014), pp. 337–365.
- [21] L. M. LUI, T. W. WONG, P. THOMPSON, T. CHAN, X. GU, AND S.-T. YAU, *Compression of surface registrations using beltrami coefficients*, in *2010 IEEE Computer Society Conference on Computer Vision and Pattern Recognition*, IEEE, 2010, pp. 2839–2846.
- [22] L. M. LUI, T. W. WONG, P. THOMPSON, T. CHAN, X. GU, AND S.-T. YAU, *Shape-based diffeomorphic registration on hippocampal surfaces using beltrami holomorphic flow*, in *International Conference on Medical Image Computing and Computer-Assisted Intervention*, Springer, 2010, pp. 323–330.
- [23] L. M. LUI, T. W. WONG, W. ZENG, X. GU, P. M. THOMPSON, T. F. CHAN, AND S.-T. YAU, *Optimization of surface registrations using beltrami holomorphic flow*, *Journal of scientific computing*, 50 (2012), pp. 557–585.
- [24] L. M. LUI, W. ZENG, S.-T. YAU, AND X. GU, *Shape analysis of planar multiply-connected objects using conformal welding*, *IEEE transactions on pattern analysis and machine intelligence*, 36 (2013), pp. 1384–1401.
- [25] T. W. MENG, G. P.-T. CHOI, AND L. M. LUI, *Tempo: Feature-endowed teichmüller extremal mappings of point clouds*, *SIAM Journal on Imaging Sciences*, 9 (2016), pp. 1922–1962.
- [26] D. QIU AND L. M. LUI, *Inconsistent surface registration via optimization of mapping distortions*, *Journal of Scientific Computing*, 83 (2020), pp. 1–31.
- [27] C. Y. SIU, H. L. CHAN, AND R. L. MING LUI, *Image segmentation with partial convexity shape prior using discrete conformality structures*, *SIAM Journal on Imaging Sciences*, 13 (2020), pp. 2105–2139.
- [28] C. WEN, D. WANG, L. SHI, W. C. CHU, J. C. CHENG, AND L. M. LUI, *Landmark constrained registration of high-genus surfaces applied to vestibular system morphometry*, *Computerized Medical Imaging and Graphics*, 44 (2015), pp. 1–12.
- [29] C. P. YUNG, G. P. CHOI, K. CHEN, AND L. M. LUI, *Efficient feature-based image registration by mapping sparsified surfaces*, *Journal of Visual Communication and Image Representation*, 55 (2018), pp. 561–571.
- [30] R. ZAYER, C. ROSSL, AND H.-P. SEIDEL, *Discrete tensorial quasi-harmonic maps*, in *International Conference on Shape Modeling and Applications 2005 (SMI'05)*, IEEE, 2005, pp. 276–285.
- [31] W. ZENG, L. MING LUI, AND X. GU, *Surface registration by optimization in constrained diffeomorphism space*, in *Proceedings of the IEEE Conference on Computer Vision and Pattern Recognition*, 2014, pp. 4169–4176.
- [32] D. ZHANG AND K. CHEN, *A novel diffeomorphic model for image registration and its algorithm*, *Journal of Mathematical Imaging and Vision*, 60 (2018), pp. 1261–1283.
- [33] D. ZHANG, X. CHENG TAI, AND L. M. LUI, *Topology- and convexity-preserving image segmentation based on image registration*, *Applied Mathematical Modelling*, 100 (2021), p. 218.

- [34] D. ZHANG, G. P. CHOI, J. ZHANG, AND L. M. LUI, *A unifying framework for n -dimensional quasi-conformal mappings*, SIAM Journal on Imaging Sciences, 15 (2022), pp. 960–988.
- [35] D. ZHANG AND L. M. LUI, *Topology-preserving 3d image segmentation based on hyperelastic regularization*, Journal of Scientific Computing, 87 (2021), pp. 1–33.
- [36] D. ZHANG, A. THELJANI, AND K. CHEN, *On a new diffeomorphic multi-modality image registration model and its convergent gauss-newton solver*, Journal of Mathematical Research with Applications, 39 (2019), pp. 633–656.
- [37] M. ZHANG, F. LI, X. WANG, Z. WU, S.-Q. XIN, L.-M. LUI, L. SHI, D. WANG, AND Y. HE, *Automatic registration of vestibular systems with exact landmark correspondence*, Graphical models, 76 (2014), pp. 532–541.